



How a river submerges into the sea: a geological record of changing a fluvial to a marine paleoenvironment during early Holocene sea level rise

D.A. HEPP,^{1*}  O.E. ROMERO,¹ T. MÖRZ,¹ R. DE POL-HOLZ² and D. HEBBELN¹ 

¹MARUM – Center for Marine Environmental Sciences and Faculty of Geosciences, Leobener Str. 8, Bremen, D-28359, Germany

²Centro de Investigación GAIA-Antarctica (CIGA), Universidad de Magallanes, Punta Arenas, Chile

Received 14 November 2018; Revised 25 June 2019; Accepted 4 September 2019

ABSTRACT: Coastal seas, and in particular estuarine systems, were significantly affected by Quaternary sea level changes. Furthermore, the dynamics of shelf and coastal evolution have had a strong impact on coastal landscapes inhabited by humans. The postglacial evolution of the vast North Sea shelf with its huge drainage systems, e.g. the Elbe Paleovalley and its tributary system, is an excellent research target to understand how coastal shelf environments change in response to sea level rise. In this study, we investigate infill sediments of the Paleo-Ems valley – a drowned extension of the modern Ems River and part of the Elbe Paleovalley drainage system. Radiocarbon-dated transgression sequences provide several new observations regarding the mode and rate of the river system submerging due to the Holocene transgression. Thus, the Paleo-Ems valley submerged within a short time span of ~200 years since the river was not able to adjust its gradient to the rapid rising sea level. The fate of the Paleo-Ems is exemplary for the rapid change of a former fluvial landscape into a coastal landscape and finally into a submarine seascape. © 2019 The Authors. *Journal of Quaternary Science* Published by John Wiley & Sons Ltd.

KEYWORDS: coastal evolution; Holocene transgression; paleolandscape; submerged river.

Introduction

Changes in sea level driven by climate variability control the dynamic development of coastal seas, which has had fundamental impacts on human settling strategies in coastal regions, especially in the youngest geological history (Nicholls and Cazenave, 2010; Harff *et al.*, 2016). Since the Last Glacial Maximum (LGM), the paleolandscape, which now forms the North Sea seafloor, has been drastically reshaped by glacial ice sheet coverage and periglacial processes and finally drowned by the postglacial sea level rise (Vink *et al.*, 2007; Peeters and Cohen, 2014; Phillips *et al.*, 2017). The rising sea level converted wide parts of coastal lowlands, partly known as Doggerland (Fig. 1; Ehlers, 2011), to shelf and coastal seas. Especially the Elbe Paleovalley (EPV) played a significant role in the postglacial North Sea setting. The EPV is a large valley structure, which drained vast coastal lowlands throughout the Weichselian until it was drowned by the advancing North Sea during the Holocene transgression (Hallik, 1962; Figge, 1980; Coles, 2000; Clarke, 2009; Özmaral, 2017).

Early studies on the development of the EPV since the LGM (Figge, 1980; Streif *et al.*, 1983) have been recently extended by a comprehensive study about the postglacial transgression into the EPV using sediment echosounder and high-resolution seismic records as well as sediment cores (Özmaral, 2017). Recent studies indicate that the EPV might have been part of a vast ice-dammed lake, which developed during the LGM (Hjelstuen *et al.*, 2017; Özmaral, 2017; Phillips *et al.*, 2018). At the end of the last glaciation, the EPV drained meltwater from the east, from the Fennoscandian Ice Shield along its southern margin, and the German low mountain range in the south across the periglacial paleolandscape towards the

North Sea (Ehlers, 2011; Özmaral, 2017). Özmaral (2017) demonstrated that pre-transgression sediment deposits within the EPV were almost eroded, with the exception of infill sediments from a channel network, which veined the valley plain from south to north. With rising sea level, the EPV was subject to at least three infill phases, in response to different sea level highstands and changes in the current regime (Özmaral, 2017). Based on relative sea level index points from the German Bight and adjacent areas as well as from Northwest German coastal areas, Vink *et al.* (2007) demonstrated that the postglacial paleolandscape in this area started to submerge at about 10 600 cal a BP and the entire landscape including the EPV was largely drowned at about 4400 cal a BP.

During the LGM sea level lowstand, the EPV was fed by various larger and smaller rivers as indicated by the paleovalleys of the modern Weser, Ems, and Eider Rivers (Fig. 1) as well as by now-lost rivers or channel networks which drained the Dogger Bank (Warnke *et al.*, 2014; Hepp *et al.*, 2017). The Elbe and Weser Rivers are thought to be the main feeders of the EPV (Figge, 1980). The Elbe River reflects the onshore part of the EPV system (Ehlers, 2011). The Weser River is a relict of the chronologically older Weser Paleovalley, which had drained the meltwaters from the Elsterian and Saalian ice shields toward the west and since the Middle Saalian, towards the EPV (Meyer, 1983). Unfortunately, due to massive Holocene sediment remobilisation in the Elbe and Weser estuaries, a direct linkage of the Weser Paleovalley to the EPV cannot be confirmed.

Based on geophysical records, Tietze (1983) identified a 2–3-km-wide paleo river valley, which discharged Weichselian meltwaters from the Jutland Peninsula toward the eastern flank of the EPV. Landward, this valley structure can be linked to the Weichselian and present-day Eider River (Fig. 1). Along the western flank of the EPV, two tributary systems are known: the Entenschnabel river system in the northern part of the EPV,

*Correspondence: D.A. HEPP, as above.

E-mail: dhepp@marum.de



Figure 1. Synthetic map of the present-day German Bight in the North Sea with a land-sea distribution reflecting the situation at $\sim 11\,000$ cal a BP with the paleocoastline being based on the -50 m bathymetric contour line (modified from Warnke *et al.*, 2014). Present day coastlines are indicated by the thin dark lines. The supposed extent of large valley structures, like the EPV, is marked in light blue. The EPV and its tributaries (Elbe, Weser, Eider and Ems Rivers) were draining the then exposed coastal lowlands also known as Doggerland (Gaffney *et al.*, 2009). The Entenschnabel river system south of the eastern Dogger Bank is marked in red. The red square marks the study area along the lower reaches of the Ems paleovalley (see Fig. 2). [Color figure can be viewed at wileyonlinelibrary.com]

and the Paleo-Ems in the southern part (Hepp *et al.*, 2012; Warnke *et al.*, 2014; Hepp *et al.*, 2017; Fig. 1). The Entenschnabel river system drained the Dogger Bank to the southeast. The system was influenced by postglacial sea level rise and developed from a single deep valley, which may initially have originated during the last glacial, to a network of shallower rivers and tributaries (Hepp *et al.*, 2017). The morphology of this network is similar to river structures known from the western part of the Dogger Bank (Fitch *et al.*, 2005; Phillips *et al.*, 2018). The Paleo-Ems is the drowned extension of the modern Ems River (Fig. 2(a)) that discharged into the southern part of the EPV during late Weichselian and the early

Holocene (Warnke *et al.*, 2014), together with the Elbe, Weser and Eider Rivers. In addition to these five documented tributaries of the EPV, it is expected that many more fluvial systems drained the late glacial and postglacial Doggerland during sea level lowstands.

While the pathways of some tributaries of the EPV are well documented in the geophysical record, only a little is known about the impact of the Holocene sea level rise on the depositional regime of the tributaries, particularly the rates of siltation and salinisation and not least the time which was needed to inundate a tributary valley to become a shallow shelf environment. The impact of the Holocene transgression

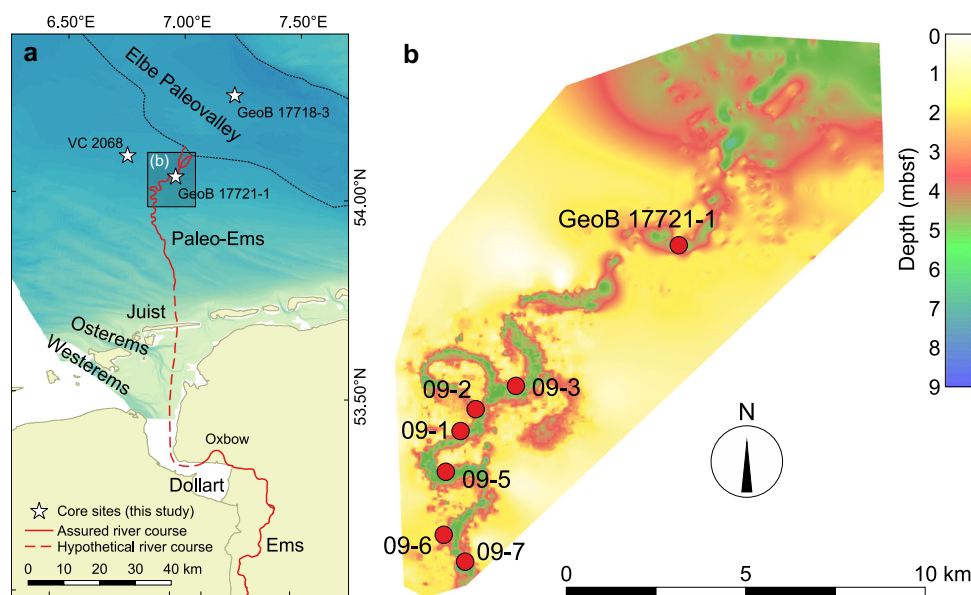


Figure 2. Location of cores used in the study area (Modified from Hepp *et al.*, 2017): (a) assured river course of the drowned late Weichselian/early Holocene Paleo-Ems valley and the modern Ems River (solid red lines) in relation to the Elbe Paleovalley (dotted black line). The hypothetical course (dashed red line) crosses today's barrier island Juist, which only was formed after the submergence of the Paleo-Ems; (b) seismic visualization of the sediment thickness above the paleosurface and the valley base. [Color figure can be viewed at wileyonlinelibrary.com]

on the depositional regime of the Paleo-Ems valley and its interconnection to the EPV is an ideal case study to understand how coastal lowland rivers respond to Holocene sea level rise. Based on sediment cores taken from the formerly mapped Paleo-Ems valley (Hepp *et al.*, 2012; Warnke *et al.*, 2014; Hepp *et al.*, 2017) and the EPV (Özmaral, 2017), we discuss the topographical and chronological relationship between the developments of the Paleo-Ems tributary, the EPV, and the surrounding landscape. Radiocarbon ages coupled with grain size distribution, organic carbon content and micropaleontological records from Core GeoB17721-1 provide insights into (i) the timing and duration of the inundation of the Paleo-Ems, into (ii) changes in the transport energy regime during the Holocene transgression as well as into (iii) changes in the paleoenvironmental setting shifting from fluvial to marine conditions, with the latter being reflected by changes in the diatom assemblage over time providing an insight on grade and rate of salinisation in the estuarine environment.

Since these processes are not only phenomena of the past, this study also aims to contribute to the understanding of the implications of sea level rise on modern coastal lowland rivers. For example, the modern Ems River is presently affected by enhanced mud aggradation induced by sea level rise, changes in tidal dynamics, and human interference in the river system. The installation of tide locks and intensive dredging are presently the only temporary successful measures to prevent the estuarine river system from siltation caused by a disequilibrium of ebb and flood tide currents, channel depth decrease and upstream shift of the channel mouth (de Jonge *et al.*, 2014).

Database and methods

This study mainly focuses on the 5.8-m-long sediment core GeoB17721-1 (located at 54°03.031' N, 06°58.585' E), which was recovered from the infill of the Paleo-Ems valley near its confluence with the EPV (Fig. 1 and Fig. 2(a)). Grain size distributions, organic carbon content and diatom assemblages were used to reveal the sedimentary and environmental response of the Paleo-Ems estuary to deglacial sea level rise. Six additional sediment cores (cores 09-1 to 09-3, and 09-5 to 09-7) were taken further upstream in the river valley (Fig. 2(b)) and the sedimentology documented. From all the cores, radiocarbon ages obtained on basal peat sequences of the infill of the Paleo-Ems valley were used to specify the timing and development of the submergence of the Paleo-Ems and the chronology of the transgression phase of the EPV (Table 1). In order to connect the results from the Paleo-Ems with the infill of the valley incision at the base of the EPV, we used the radiocarbon-dated sediment record from core GeoB17718-3 provided by Özmaral (2017).

Sediment samples

Sediment core GeoB17721-1 was obtained in a water depth of 30.5 m, during RV Heincke expedition HE405 in 2013 using a Geo-Corer 6000 Vibrocoring System with 28 Hz vibromotor and a barrel length of 5.80 m. On board, the core was split, photographed, and the lithological and sedimentary characteristics were documented. Additionally, samples were taken from basal peat intervals from sediment cores 09-x, located approximately 8.5–20.4 km southwest of core GeoB17721-1 and in the upstream direction of the Ems paleovalley (Fig. 2(b)). The exact coordinates cannot be given here due to commercial restriction. These cores were recovered in 2009 from water depths between 28.7 and 31.1 m. All cores provide sample

material from the infill of the Paleo-Ems valley (see Hepp *et al.*, 2017).

Grain size analyses

A total of 25 samples from core GeoB17721-1 with a sampling space of about 20 cm were analysed for their grain size distribution using a Beckman Coulter Laser Diffraction Particle Size Analyzer LS 13320. The measurements were taken at the Particle Size Laboratory at MARUM, University of Bremen. Prior to the measurements, the terrigenous sediment fractions were isolated by removing organic carbon, calcium carbonate, and biogenic opal. The obtained results provide the particle size distribution of a sample from 0.04 to 2000 µm divided into 116 size classes and is given in volume percentage (vol%). The average standard deviation integrated over all size classes is better than ± 4 vol%. The grain size frequencies were processed using the GRADISTAT 8.0 software to obtain particle size summary parameters (Blott and Pye, 2001).

Organic carbon and sulfur contents

Carbon and sulfur content was determined using the automated C-S analyser Multi EA 4000 (Analytik Jena AG). Fifty-one samples from core GeoB17721-1 were freeze-dried and pulverised. To obtain the total organic carbon (TOC) content, 10% HCl was added to 300 mg of sample material to digest the total inorganic carbon. The analysis of the decalcified material in the C-S analyser provided TOC and total sulfur (TS) content in weight percentage (wt%).

Radiocarbon ages and age conversion

Hand-picked plant macrofossils (peat or plant remains) or marine calcareous fossils (mainly foraminifera and shell valves or their fragments) from 22 samples, as well as one well-preserved but possibly reworked shell valve were dated using accelerator mass spectrometry ¹⁴C dating. Radiocarbon ages of samples from core GeoB17721-1 were determined at the Poznań Radiocarbon Laboratory (Poznań, Poland), whereas radiocarbon ages from peat layers or layers of decayed organic matter in cores 09-x were determined at the W. M. Keck Carbon Cycle Accelerator Mass Spectrometry Laboratory (University of California, Irvine) (see Table 1 for details). All radiocarbon dates were converted to calendar ages using the CALIB 7.0 program (Stuiver and Reimer, 1993; <http://calib.org>). The reservoir effect of the marine samples was corrected with ΔR values provided by Scourse *et al.* (2012) for the German Bight (mean $\Delta R = 83$), with the restriction that the ΔR values were determined on post-industrial samples. For comparison, the external age dates provided by Özmaral (2017; see GeoB17718-3) and Vink *et al.* (2007) used in this study were recalibrated accordingly. All calibrated radiocarbon ages are given as cal a BP. The median of the probability distribution of the σ_2 range is used as a reliable estimation of the sample's calendar age.

Diatom assemblages

The study of the diatom assemblage was carried out on 15 samples, spaced at every 20 cm of core GeoB17721-1. Samples were prepared according to the standard randomly distributed microfossil method of Schrader and Gersonde (1978). Qualitative and quantitative analyses were carried out on permanent slides of acid-cleaned material (Naphrax® mounting medium) at 1000x magnification using a Zeiss® Axioscop (MARUM, University Bremen, Germany). We used the counting methodology of valves proposed by Schrader and

Table 1. Accelerator mass spectrometry (AMS) radiocarbon dates and calibrated ages of sites used in this study. Radiocarbon dates of GeoB17718-3 were recalibrated from dates provided by Özmaral (2017).

Lab No.a	Core ID	Depth in core (cm)	Material	¹⁴ C a BP	σ1 range (cal a BP)	σ2 range (cal a BP)	Median σ1 (cal a BP)	Median σ2 (cal a BP)
Poz-83150	GeoB17718-3	531–532.5	Plant remains	9510 ± 50	10 695–11 067	10 600–11 085	10 984	10 770
Poz-93829	GeoB17721-1	30–31	Marine shells	6880 ± 40	7276–7371	7245–7409	7324	7327
Poz-93830	GeoB17721-1	61–62	Marine calcareous fossils	7060 ± 60	7423–7527	7372–7582	7475	7477
Poz-93763	GeoB17721-1	141–142	Plant remains	16 580 ± 90	19 872–20 139	19 707–20 267	20 006	19 987
Poz-87002	GeoB17721-1	151–152	Plant remains	8300 ± 50	9258–9421	9133–9440	9340	9287
Poz-87003	GeoB17721-1	261–262	Plant remains	8400 ± 50	9326–9488	9302–9518	9445	9410
Poz-87004	GeoB17721-1	381–382	Plant remains	8450 ± 50	9450–9520	9324–9538	9485	9470
Poz-93765	GeoB17721-1	402.5–403.5	Plant remains	8720 ± 50	9560–9737	9550–9887	9649	9691
Poz-83151	GeoB17721-1	476.5–477.5	Peat	9970 ± 50	11 270–11 599	11 248–11 693	11 340	11 436
UCIAMS 84362	Core 09-1	439.5–441	Peat	8940 ± 25	9949–10 191	9925–10 197	10 030	10 049
UCIAMS 79098	Core 09-1	480–481.5	Peat	9965 ± 25	11 288–11 399	11 266–11 601	11 343	11 478
UCIAMS 79100	Core 09-2	500–501.5	Peat	9910 ± 25	11 252–11 311	11 241–11 387	11 281	11 300
UCIAMS 84359	Core 09-3	336–337.5	Peat	8555 ± 25	9526–9542	9499–9547	9534	9523
UCIAMS 79101	Core 09-3	361.5–363	Peat	9620 ± 20	10 868–11 123	10 791–11 148	11 010	11 015
UCIAMS 79105	Core 09-5	276–277	Peat	8785 ± 20	9736–9887	9701–9898	9830	9799
UCIAMS 79106	Core 09-5	499–500	Peat	9585 ± 25	10 788–11 082	10 770–11 095	10 985	10 932
UCIAMS 79107	Core 09-6	544–545.5	Peat	8825 ± 20	9780–10 106	9736–10 119	9854	10 003
UCIAMS 84357	Core 09-6	610–612	Peat	9270 ± 25	10 420–10 509	10 301–10 562	10 464	10 469
UCIAMS 84358	Core 09-6	621.5–623	Peat	9530 ± 25	10 732–11 064	10 711–11 070	10 985	10 892
UCIAMS 79108	Core 09-6	678–679	Peat	10 000 ± 25	11 356–11 601	11 318–11 614	11 462	11 466
UCIAMS 79109	Core 09-7	318.5–320	Peat	8315 ± 20	9299–9402	9279–9425	9335	9352
UCIAMS 84743	Core 09-7	358.5–360	Peat	9710 ± 25	11 154–11 198	11 107–11 205	11 176	11 156
UCIAMS 79110	Core 09-7	405–407	Peat	10 100 ± 70	11 409–11 930	11 354–12 005	11 514	11 697

^aRadiocarbon laboratory: Poz = Poznań Radiocarbon Laboratory (Poland); UCIAMS = W. M. Keck Carbon Cycle Accelerator Mass Spectrometry Laboratory (University of California, Irvine).

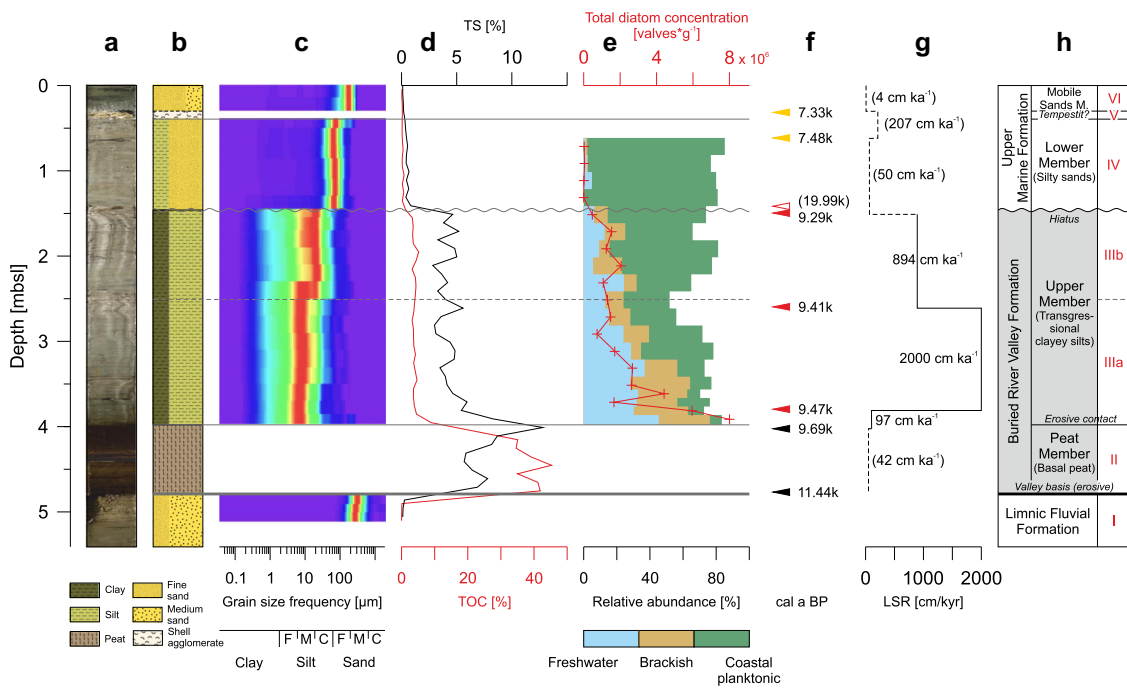


Figure 3. Sedimentological data of core GeoB17721-1 from the Paleo-Ems valley. From left to right: (a) stitched core image with non-scale width; (b) lithological column resulting from core description (legend at the base of the figure); (c) frequency plot of the grain size distribution (F = fine, M = medium, C = coarse), the peat and shell layers were not analysed; (d) total organic carbon content (TOC, red line) and total sulfur content (TS, black line); (e) relative diatom abundance (%) of three main groups: into freshwater, brackish and coastal planktonic (marine) species, as well as total diatom concentration (valves/gr; red line); (f) calibrated radiocarbon ages (see Table 1). The colours refer to the type of the dated material (yellow = marine calcareous fossils or shells, red = plant remains, black = peat); (g) calculated linear sedimentation rates (LSR). For the reworked sands Units IV to VI we can provide only apparent depositional rates; (h) stratigraphic interpretation of the lithological Units I–VI (red) (see text). The stratigraphical formation names are provided by Coughlan *et al.* (2018). [Color figure can be viewed at wileyonlinelibrary.com]

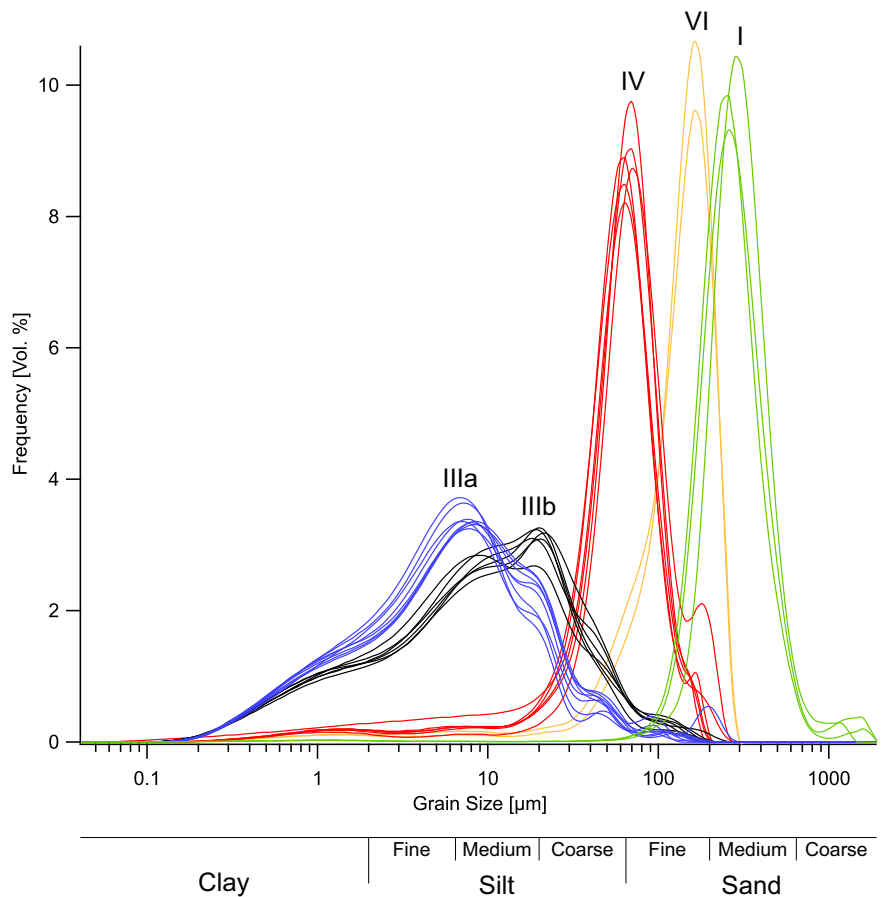


Figure 4. Grain size distributions of the samples from core GeoB17721-1. The colours correspond to Units I, III, IV and VI (see text). [Color figure can be viewed at wileyonlinelibrary.com]

Gersonde (1978). Several traverses across each cover slip were examined, depending on diatom abundances (between 250 and 400 valves were counted for each cover slip). Two cover slips per sample were scanned in this way.

Results

Core description and grain size analysis

Sediment core GeoB17721-1 penetrated the base of the Ems paleovalley and comprises the whole infill of the valley and the overlying sediments. Based on colour, lithological contacts, sediment composition, and the grain size distributions, the core can be divided into six units (Fig. 3 and Fig. 4). In the following, the units are described from bottom to top:

Unit I (541–479 cm) is mainly composed of over-consolidated dark greyish brown medium sand (~78 vol%) with some fine sands (~18 vol%). The mean median grain size (D_{50}) is 991 μm . The sediment is moderately sorted, devoid of any shell fragments and contains tiny particles of dark organic matter. The skewness is fine skewed and the kurtosis mesokurtic (Fig. 4). The upper contact to Unit II is erosive.

Unit II (479–398 cm) is a very dark brown peat interval. The peat is quite stiff and shows internal stratification. Larger plant fragments were not observed, but plant fibres, seeds and pollen are well preserved. This unit was not sampled for particle size measurements. The upper contact to Unit III is erosive.

Unit III (398–146 cm) is composed of very dark greenish-grey, poorly-sorted clayey silt (average total silt content: 78 vol%; average total clay content: 20 vol%; mean D_{50} = 24 μm). The sediment is stratified with very thin layers of dark organic matter derived from plant and root fragments. A shift from fine to coarse silt at about 250 cm core depth coincides with a prominent change in linear sedimentation rates (LSR; see section 3.3 below) and divides subunits IIIa and IIIb. For subunit IIIa the mean D_{50} is 20 μm , the skewness is symmetrical to fine skewed and the kurtosis mesokurtic (Fig. 4). For Unit IIIb the mean D_{50} is 29 μm , the skewness is fine skewed and the kurtosis platykurtic. The upper contact to Unit IV is erosive.

Unit IV (146–40 cm) is composed of dark greenish-grey, poorly-sorted silt to fine sands with shell fragments (average total coarse silt content: 49 vol%; average total fine sand content: 48 vol%; mean D_{50} = 189 μm), with a slight coarsening upward. The skewness is fine skewed and the kurtosis mesokurtic to platykurtic (Fig. 4). The upper contact to Unit V is erosive.

Unit V (40–30 cm) describes an agglomeration of well-preserved shell valves and shell fragments (<2 cm large) of the families Cardiidae and Myidae. Both are coastal species typical of the modern North Sea. The erosive lower contact and the formation as a thick layer suggests a deposition of reworked shells during a single high-energy event or over a short time period. The upper contact to Unit VI is gradational.

Unit VI (30–0 cm) is mainly composed of poorly-sorted fine sand (av. 70 vol%) to medium sand, interspersed with shell fragments. The mean D_{50} is 369 μm , the skewness is symmetrical and the kurtosis is very leptokurtic (Fig. 4).

The additional cores 09-x were first presented by Hepp *et al.* (2017). They show a similar lithologic stratigraphy to GeoB17721-1 (Fig. 6): Medium sands are overlain by peat intervals and the transitions of the peat interval are erosive. In contrast to GeoB17721-1, cores 09-5 and 09-7 show additional peat layers, which are intercalated with fine sandy silts or silty fine sands. The peat sequence is often overlain by clayey silts (cores 09-1, 09-3, and 09-6), again overlain by fine

sandy silts. The top of the cores is composed of fine sands (cores 09-2, 09-3, 09-6, and 09-7). Core 09-5 shows a similar shell layer to that described for Unit V in core GeoB17721-1.

Organic carbon and sulfur contents

The TOC content of core GeoB17721-1 is consistent with the established lithological units (Fig. 3(d)). Very high TOC content of 35–45 wt% characterises the peat (Unit II). In the clayey silts (Unit III), the TOC content decreases within the first ten centimetres above Unit II to a constant level of 3.3–5.0 wt%. However, the TOC seems to be more constant in Unit IIIb than in Unit IIIa. The lowest TOC content of 0.1–1.0 wt% was observed in sandy units (Unit I, IV, and VI) making up the base and the top of the core.

The TS content exhibits a similar pattern as the TOC content; however, with much lower values. Unit II has a TS content of 5.7–8.7 wt% and shows an upward-increasing trend, reaching a maximum of 12.8 wt% at the transition to Unit III. In the clayey silts (Unit III) the TS content varies between 2.8–5.9 wt%, whereas in the sands (Unit I, IV, and VI) the TS content is always <0.8 wt%.

The TOC/TS ratio is very high with values of 4.2–8.0 in the peat section (Unit II) and ranges between 0.7 and 1.3 in the silty clay section (Unit III), and most parts of the sand sections (Units I, IV and VI). Only in the uppermost 30 cm, the youngest sediments of Unit VI above the shell layer, the ratio increases up to 2.0–2.3. The TOC–TS scatter plot shows clear clusters for each unit (Fig. 5). The TOC/TS ratios of the sand and silty sand sections (Units I, IV, VI) fall mainly within the range of normal marine siliciclastic sediments ($\text{TOC}/\text{TS} = 2.8 \pm 0.8$) as proposed by Morse and Berner (1995) for weight ratios of organic carbon to pyrite sulfur. The TOC/TS ratios of the silty clay sections (Unit III) point to more suboxic conditions. However, these findings have to be handled with some caution, because determining factors like rates of aerobic and anaerobic metabolism in the sediment or burial rates have not been considered so far.

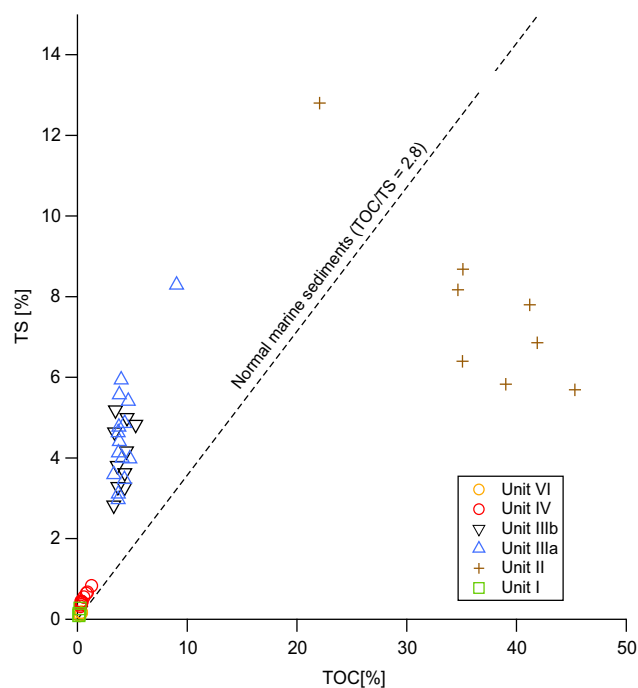


Figure 5. Relationship between total sulfur (TS) content and total organic carbon (TOC) content (according to Berner and Raiswell, 1984) for samples studied from core GeoB17721-1. The colors correspond to Units I–IV and VI (see text). [Color figure can be viewed at wileyonlinelibrary.com]

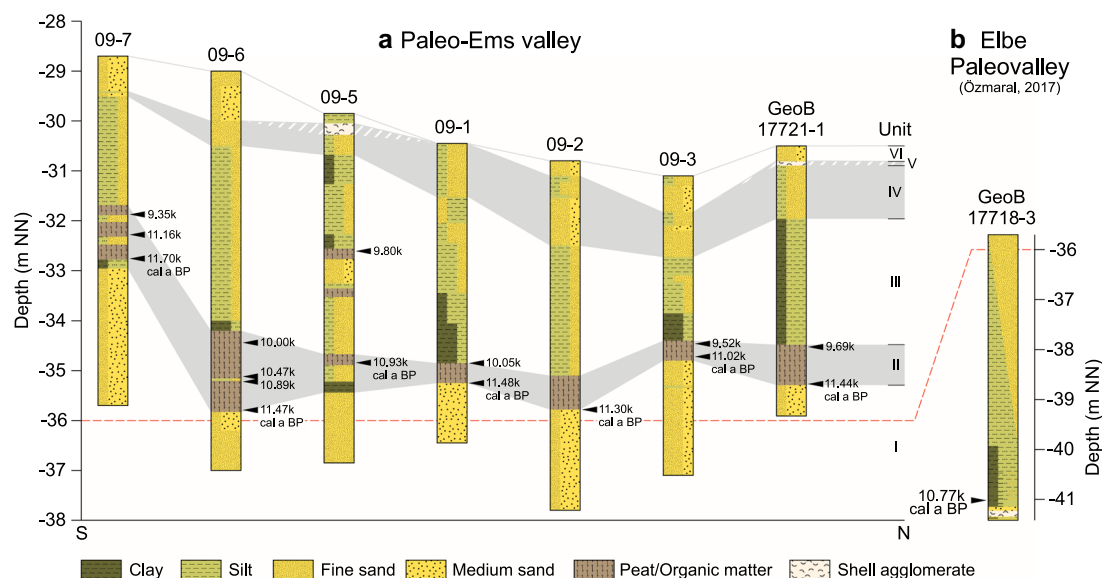


Figure 6. Lithological columns (a) from the Paleo-Ems valley with radiocarbon ages from peat intervals (cores 09-1 to 09-3, 09-5 to 09-7 and GeoB17721-1), and (b) from an incision at the base of the EPV with radiocarbon age from plant fragments (core GeoB17718-3; see Özmaral, 2017). All core depths are adjusted to the 1-m-bathymetric dataset provided by the project “Geopotenzial Deutsche Nordsee” (<https://www.gpdn.de>). Radiocarbon ages are given in Table 1. [Color figure can be viewed at [wileyonlinelibrary.com](https://onlinelibrary.com)]

Radiocarbon ages and linear sedimentation rates

Eight radiocarbon ages obtained on core GeoB17721-1 provide information on the timing of valley infill and the deposition of the overlying sediments (Table 1 and Fig. 3(f)). Bases and tops of the peat section (Unit II), the clayey silt section (Unit III) and the overlying sands (Units IV–VI) were selected for radiocarbon dating. According to the resulting ages, peat growth started at about 11 440 cal a BP (477 cm core depth), which is equivalent to the beginning of the early Holocene. The youngest age obtained from the uppermost part of the peat section is 9690 cal a BP (403 cm core depth). Due to the assumed hiatus at the transition to Unit II, it is not possible to determine the exact termination of this section.

The clayey silt section (Unit III) started at about 9470 cal a BP (381 cm core depth). The youngest age obtained for this unit is 9290 cal a BP (151 cm core depth). Hence, the sediments of Unit III were deposited quickly with $\sim 1260 \text{ cm ka}^{-1}$ over a very

short time span of about 180 years. An additional dating of 9410 cal a BP (261 cm core depth) might point to a prominent drop in LSR within Unit III with $\sim 2000 \text{ cm ka}^{-1}$ in Unit IIIa and $\sim 894 \text{ cm ka}^{-1}$ in Unit IIIb. However, the short time span between the oldest and youngest ages of Unit III is subject to some uncertainty with respect to the error ranges of the dating (Table 1). Nevertheless, a shift in the grain size distribution at the same depth (Fig. 3(c)) implies that a change in the sedimentary regime probably also results in a shift in LSR. The remarkably high age of 19 990 cal a BP determined on plant remains found at 141.5 cm core depth does not fit the age model based on the remaining seven radiocarbon ages. The sample was taken directly above the prominent hiatus at the transition from Unit III to Unit IV (Fig. 3) and, thus, might be affected by reworked material. Consequently, this dating has not been considered further.

The sand Unit IV spans from somewhat after 9290 cal a BP (considering the hiatus) to 7480 cal a BP (61 cm core depth),

Table 2. Total diatom concentration and relative abundance (%) of diatom groups in core GeoB17721-1.

Lithol. Unit	Depth in core (cm)	Total diatom concentration (valves * g ⁻¹)	Diatom abundance (%)		
			Freshwater	Brackish	Marine coastal planktonic
IV	71.5	30 133	1	1	83
IV	91.5	53 332	2	1	74
IV	111.5	20 323	5	0	75
IV	131.5	5 262	0	0	81
IIIb	151.5	475 866	6	8	59
IIIb	171.5	1 534 795	13	12	41
IIIb	191.5	1 241 609	9	6	66
IIIb	211.5	2 058 346	6	17	54
IIIb	231.5	1 075 855	24	8	33
IIIa	251.5	1 307 007	13	11	28
IIIa	271.5	1 480 467	15	13	28
IIIa	291.5	741 518	24	15	32
IIIa	311.5	1 710 629	29	6	44
IIIa	331.5	2 674 432	37	20	16
IIIa	351.5	2 637 449	28	36	13
IIIa	361.5	4 410 397	33	30	8
IIIa	371.5	1 668 816	32	24	20
IIIa	381.5	5 953 426	30	33	10
IIIa	391.5	8 004 926	45	31	7

which results in a minimum estimate for the LSR of 50 cm ka⁻¹. Based on the radiocarbon ages, the agglomeration of well-preserved valves and shell fragments (Unit V) was deposited roughly between 7480 cal a BP and 7330 cal a BP (30 cm core depth). Assuming the modern sea floor was completely recovered in the sediment core, we calculate a deposition rate of about 4 cm ka⁻¹ for the uppermost Unit VI.

In addition, basal and intercalated peat layers as well as layers of highly decayed organic matter from the additional six cores 09-x were sampled for radiocarbon age dating (Table 1 and Fig. 6(a)). The radiocarbon ages at the base of the basal peat layers range between 11 700 cal a BP and 11 020 cal a BP, matching the beginning of peat growth documented for core GeoB17721-1. The youngest radiocarbon ages of the basal and intercalated peat sequences range between 10 050 cal a BP and 9350 cal a BP, also matching the data obtained on core GeoB17721-2.

Diatom content and composition of the assemblage

The total diatom concentration in core GeoB17721-1 ranges between 4.8×10^5 and 8.0×10^6 valves g⁻¹ (average = $2.5 \times 10^6 \pm 1.7 \times 10^7$ valves g⁻¹). Values are highest between 9690 and 9470 cal a BP and strongly decrease upward in the core (Fig. 3(e), Table 2). The diatom preservation is generally good. Valves show no significant enlargement of the areolae or evidence for any dissolution of the valve margin. This suggests rapid deposition and/or little reworking. In addition to marine diatoms, other siliceous components are silicoflagellates, radiolarians and land-derived freshwater diatoms or phytoliths (silica bodies of epidermic grass cells). In terms of number of individuals, diatoms dominate the siliceous fraction throughout core GeoB17721-1; their concentration is always one to four orders of magnitude higher than that of the above-mentioned siliceous organisms encountered (not shown here).

The diatom assemblage is diverse and contains around 90 species with the vast majority being purely marine or brackish/intertidal, while 18 of them are fully freshwater diatoms (Table 3). The marine diatom community is dominated by coastal planktonic and brackish species. Coastal planktonic diatoms thrive in neritic, oligo-to-mesotrophic waters with high to moderate dissolved silica levels, becoming more abundant during intervals of weak turbulence and responding mainly to moderate upwelling (Romero and

Armand, 2010; Crosta *et al.*, 2012). Main components of the brackish group mostly live attached to a substratum as epipellic, epiphytic or epizoic diatoms. The main brackish groups are *Nitzschia angulata*, *Diploneis smithii*, *Melosira nummuloides*, *Delphineis surirella* and several species of *Cymatosiraceae* (Round *et al.*, 1990). The freshwater community is dominated by species of *Aulacoseira* and *Cocconeis*, and *Navicula cincta* and *Gyrosigma scalproides* (Hartley, 1996).

In general, two main intervals are recognised in the species-specific assemblage of diatoms; between 9690 and 9470 cal a BP (beginning of Unit IIIa; Fig. 3(e) and (h)), freshwater and brackish water diatoms dominate (common contribution always exceeds 55%), whereas coastal planktonic components increase after 9470 cal a BP. This increase matches the strong decrease in the total diatom concentration (Fig. 3(e)). According to grain size, TOC and LSR data, the differentiation between Units IIIa and IIIb can also be observed in the rise in the relative abundance of coastal planktonic diatoms, more obvious in Unit IIIb than in Unit IIIa. The relative abundance of coastal planktonic diatoms increases steadily towards the top of the core and reaches its first maximum at about 210 cm core depth, which corresponds to an age of about 9380 cal a BP; based on the assumption of a constant sedimentation rate within Unit IIIb.

Discussion

Age relationship between the Ems and Elbe paleovalleys with respect to models of relative sea level rise

The core transect investigated covers the entire lower ~20 km of the Ems paleovalley (Fig. 1). The 09-x cores show a lithological valley infill succession (Hepp *et al.*, 2017) comparable to GeoB17721-1 (Fig. 6(a)): pre-river sands – basal peat formation – transgressional clays and silts with intercalated peats – sands with shell layers (possibly tempestites). Thus, basal peats or layers rich in organic matter were found in all cores investigated here. Radiocarbon ages obtained at the base of these sections define the beginning of peat growth between 11 700 and 11 020 cal a BP (Table 1 and Fig. 6). The youngest radiocarbon ages date between 9800 and 9350 cal a BP and define the termination of

Table 3. Diatom assemblage comprising a diversity of around 90 marine, brackish and freshwater species.

Freshwater diatoms	Brackish diatoms	Marine coastal planktonic diatoms
<i>Achnanthes delicatula</i>	<i>Dimmeregramma minor</i>	<i>Actinocyclus curvatus</i>
<i>Achnanthes brevipes</i>	<i>Diploneis smithii</i>	<i>Actinocyclus octonarius</i>
<i>Cyclotella ocellata</i>	<i>Navicula meniscus</i>	<i>Actinocyclus senarius</i>
<i>Gomphonema acuminata</i>	<i>Nitzschia angulata</i>	<i>Actinocyclus vulgaris</i>
<i>Hannaea</i> sp.	<i>Tryblionella hungarica</i>	<i>Adoneis pacifica</i>
<i>Hantzschia ampyoxis</i>		<i>Auliscus sculptus</i>
<i>Luticola mutica</i>		<i>Biddulphia rombhuss</i>
<i>Navicula cincta</i>		<i>Cymatosiraceae</i> spp.
<i>Navicula digitoradiata</i> var. <i>rostrata</i>		<i>Delphineis surirella</i>
<i>Nitzschia brevissima</i>		<i>Navicula peregrina</i>
<i>Nitzschia scalaris</i>		<i>Odontella aurita</i>
<i>Pinnularia</i> spp.		<i>Paralia sulcata</i>
<i>Rhopalodia</i> sp.		<i>Rhizosolenia setigera</i>
<i>Stauroneis</i> spp.		<i>Surirella brightwellii</i>
<i>Stauroneis</i> spp.		<i>Tabularia</i> sp.
<i>Surirella brebissoni</i> var. <i>kuetzingii</i>		<i>Thalassionema frauenfeldii</i>
<i>Synedra</i> spp.		<i>Thalassionema nitzschioides</i> var. <i>nitzschioides</i>
		<i>Tryblionella navicularis</i>

peat formation or the beginning of the transgressional units. Differences from core to core in unit thicknesses as well as the occurrence of intercalated peat layers (Fig. 6(a)) are most likely a consequence of different geomorphological settings along the valley, e.g. on the valley centre, valley flanks, point bars, and cut banks (Fig. 2(b)). Cores 09-5 and 09-7 exhibit intercalated peat sequences, which might be explained by common regional dislocations of the river bed in a meandering river setting (Hepp *et al.*, 2017).

The chronological relation of the Paleo-Ems valley and the EPV can be assessed with radiocarbon ages obtained from the stratigraphic oldest known infill sequences of both valleys. Özmaral (2017) provides one radiocarbon age obtained from the stratigraphically oldest known infill sequences at the base of the EPV. This infill is composed of alternating layers of dark greyish brown medium sand and an intercalated agglomeration of well-preserved and fragmented marine shells (*Cardiidae*) overlain by very dark greenish grey clayey silt, which coarsens upward to clayey fine sands with common shell, plant and wood fragments (Özmaral, 2017). The radiocarbon age was determined on plant remains taken from core GeoB17718-3 (Table 1 and Fig. 6(b)) and with 10 770 cal a BP it corresponds to the age range of the peats from the Ems paleovalley (Fig. 1). The corresponding age ranges could imply that the timing of peat growth in the Paleo-Ems valley and the drowning of the EPV are linked to the same marine flooding phase. However, the difference in elevation of more than 5 m between the bases of the EPV and the Paleo-Ems River valleys (Fig. 6 and Fig. 7) seems to contradict this assumption. A

comparison with the hydrogeological map provided by the Lower Saxony Soil Information System NIBIS® (<https://nibis.lbg.de/cardomap3/>) shows that height gradients of about 5 m for the sea-level-coupled groundwater in the coastal area onshore over a distance of few kilometres indeed occur, although these are mostly linked to impermeable strata (clays or clayey soils) below the groundwater. Although the sediments below the peat unit in the Paleo-Ems valley are composed of overconsolidated sands, clayey sediments found along the western flank of the EPV (Özmaral, 2017) could have the potential to impound the ground water. Furthermore, the greater distance of ~20 km between the Paleo-Ems valley and the EPV sites gives support to a sea level groundwater effect affecting both sites at the same time despite the observed 5 m height difference. An alternative scenario could be that the peat in or at the flanks of the Paleo-Ems valley developed on a local scale and the peat growth was independent from relative sea-level-coupled groundwater. Sea level independent post-glacial peat bogs are a well described phenomenon in the southern North Sea (Jelgersma, 1961). A local paludification can occur when the surface of the Pleistocene subsoil runs almost horizontally and groundwater accumulates in shallow depressions (Lange and Menke, 1967). However, the very good spatio-temporal fit of the inundation of the peats in the Paleo-Ems valley to the regional sea level record (see below and Fig. 7) points to the link with sea level rise and also to the onset of local peat growth.

The radiocarbon ages from the Paleo-Ems valley infill can be integrated into the relative sea level model

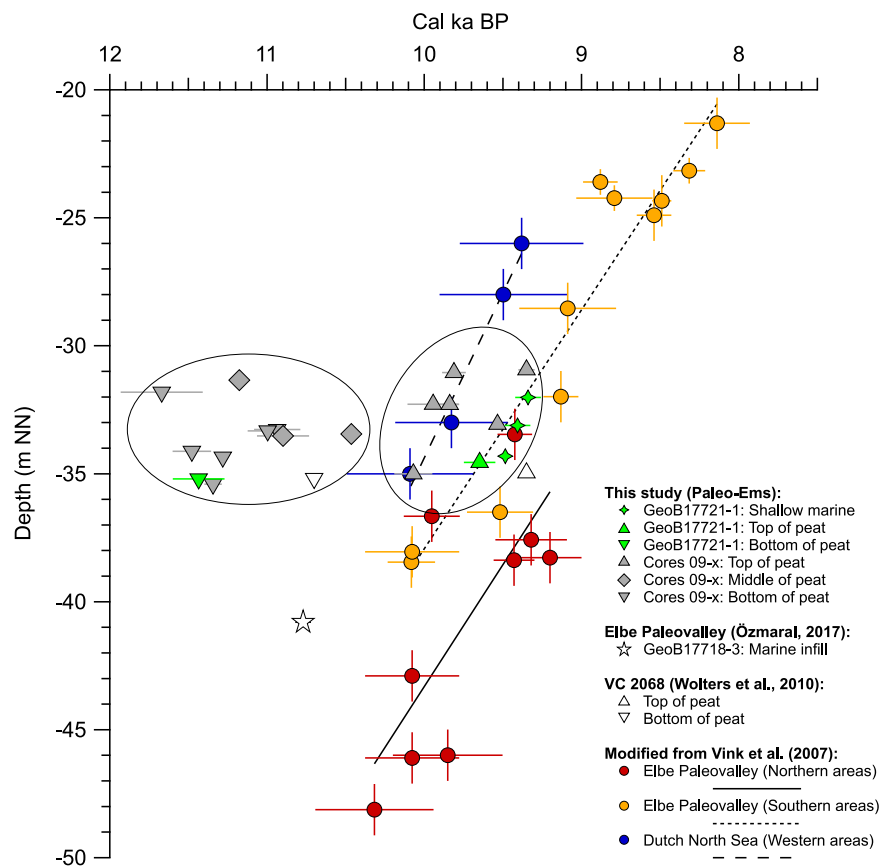


Figure 7. Age–depth relationship of sea level indicators from the southern North Sea modified from Vink *et al.* (2007; Fig. 4) complemented by radiocarbon ages resulting from this study. Colour-coded filled circles mark basal peat index points from three distinct areas in the southern North Sea (including the related linear regression lines) as indicated in the legend (Vink *et al.*, 2007): the ‘EPV (Northern areas)’ covers the area between the western and the eastern flanks of the EPV south of the Dogger Bank, the ‘EPV (Southern areas)’ is mainly congruent to the study area and extends between the southeastern flank of the EPV and the East Friesian Island Juist, and the ‘Dutch North Sea (Western areas)’ reaches from the Dogger Bank to the Oyster Grounds. Colour-coded filled triangles, diamonds and stars mark index points resulting from this study of the infill of the Paleo-Ems River valley (for details see legend). The horizontal error bars represent the σ_2 -calibrated age range of the calibrated or recalibrated radiocarbon ages; the vertical error bars correspond to the total vertical error in sample altitude. [Color figure can be viewed at wileyonlinelibrary.com]

presented by Vink *et al.* (2007; Fig. 7). The age–depth distribution of age points from core GeoB17721-1 and cores 09-1 to 09-3 and 09-5 to 09-7 shows two clearly defined groups: (1) age points from the top of peat intervals (Fig. 7, green or grey triangles facing up) match the index points, based on radiocarbon ages from basal peats, either from the areas in the southern part of the EPV (Fig. 7, yellow circles) or from the western part of the Dutch North Sea (Fig. 7, blue circles); whereas (2) the age points from the bottom or the middle of the peat intervals are significantly older (green or grey triangles facing down and grey rhombs). Ages obtained from the shallow marine, brackish or intertidal interval of core GeoB17721-1 (green diamonds), overlying the basal peat, match the index points from the southern part of the EPV (yellow circles) and, thus, reflect the flooding of the fluvial system. The age point from the marine infill of the incision at the base of the EVP (Fig. 7, white star) shows that the EPV experienced the sea level rise around 1000 years earlier than peats from the same depth (see Fig. 7, red circles) in the northern EPV area but outside of the valley. One tentative explanation would be that the EPV was topographically better connected to the advancing North Sea than other morphological depressions.

In contrast to the valley infill recovered in core GeoB17721-1, sediment core VC 2068 taken from a slightly more elevated setting approximately 15 km northwest of the lower part of the Ems paleovalley comprises early Holocene coastal mire deposits probably filling an isolated local depression (Wolters *et al.*, 2010) (Fig. 2(a)). Both cores reveal the transition from Pleistocene sands to peat formations at about 35.4 or 35.2 m water depths, which in core VC 2068 have been dated to have formed between 10 700 and 9350 cal a BP (Wolters *et al.*, 2010). This means that the onset of the peat growth in the Paleo-Ems was 600–700 years earlier (between 11 480 and 11 300 cal a BP), possibly linked to a sea-level-induced rise of the groundwater table compared with the onset of peat growth in a mire setting in the exposed landscape. Wolters *et al.* (2010) proposed that the peat growth (core VC 2068) started independent of sea level rise. However, it seems that both the valleys and the exposed landscape were inundated during the same flooding phase. The transgressive phase is documented by a gradual transition from solely freshwater-fed mire communities to brackish reed communities in the pollen diagram of VC 2068 dated to 9460–9230 cal a BP (Wolters *et al.*, 2010). A gradual transition from freshwater to marine species is observed in the composition of the diatom assemblage in core GeoB17721-1.

Sedimentation history

The reconstruction of the depositional history of the Paleo-Ems estuary is based on the combined interpretation of grain size distributions, organic carbon content, radiocarbon dating, diatom concentrations, and the composition of the diatom assemblage. In general, we distinguish between fluvial, transgressive and marine phases (see stratigraphic interpretation in Fig. 3(h)). The sediments of core GeoB17721-1 belong primarily to the Buried River Valley Formation and the Upper Marine Formation within the stratigraphic concept developed for the German North Sea sector by Coughlan *et al.* (2018).

Fluvial phase (Late Weichselian to 11 500 cal a BP)

The Paleo-Ems River probably already has a long history; for example, in Westphalia alluvial terraces of the Ems River are documented from the late Saalian and Weichselian times

(Hempel, 1963). Based on seismic data and sediment core studies, Hepp *et al.* (2017) propose that the Paleo-Ems incised into Pleistocene glaciofluvial sands at least since the LGM, thereby creating a meandering river (see also Fig. 2(b)). Also, the new core data reveals the incision of the river into Pleistocene sands. The age of the basal peat of core 09-7 (11 700 cal a BP) indicates that peat growth had already started at the end of the fluvial phase.

Perimarine phase (11 500 to 9500 cal a BP)

In core GeoB17721-1 and most of the 09-x cores, 40–160 cm-thick basal peat layers directly overlie the valley base, formed by earlier fluvial erosion processes. The absence of evidence of characteristic fluvial deposits suggests that the fluvial activity was restricted to a small area of the valley at this point, so that the peat could grow directly from the base. Combining all cores (except core 09-7) provides evidence for the onset of peat growth between 11 480 and 11 300 cal a BP and its termination at around 9500 cal a BP. Although there are some indications (see above) that the Paleo-Ems was coupled to groundwater via the EPV at the beginning of the perimarine phase; there is no *in situ* evidence. However, the influence of the sea level rise on the depositional regime in the Paleo-Ems valley increased and resulted in a direct control at the end of the phase.

Brackish phase (9500 to 9300 cal a BP)

Peat-growing ceased at 9500 cal a BP. After this, clay-rich muds with fine sands and high organic carbon contents dominate the sediment composition of GeoB17721-1. Rising sea level had a fundamental impact on the dynamic of the tidal regime. High sedimentation rates of 894 to 2000 cm ka⁻¹ demonstrate that the valley was silting up rapidly within a few hundred years, maybe due to an upstream shift of the coastline and/or a disequilibrium of ebb and flood tide currents (Fig. 3(g)). An upward coarsening of the very poorly sorted clayey silts just above the peat points to a slight increase in the stream competence. This upward coarsening coincides with the rapid decrease in total diatom concentration followed by the rapid replacement of fluvial-transported freshwater diatoms by brackish and marine species. However, we suppose that the siltation and salinisation were caused by a decrease of the stream capacity, since the river was not able to adjust its gradient to the rapidly rising sea level. Presently, there is no certainty as to whether the stream capacity also had a changing effect on the tidal regime. A slight jump to coarser grain sizes is seen at around 9410 cal a BP, accompanied by a further increase in the relative proportion of coastal planktonic diatoms, which become the dominant group. The transition shown in both grain size distribution and the diatom assemblage are interpreted to represent the transgressive contact, when freshwater conditions changed to a marine-influenced environment, thus resulting in brackish or coastal lagoonal conditions.

Marine phase (after 9300 cal a BP)

The exact timing of the beginning of the marine phase is not clear because of a hiatus that is indicated by the sudden distinct shift in the grain size distribution at ~150 cm core depth in GeoB17721-1. However, after 9290 cal a BP the depositional system changed to full marine conditions, as revealed by the almost complete absence of freshwater and brackish diatoms and the abrupt shift in the grain size distribution. This hiatus might be explained by the southward

shift of the coastline due to the transgression and the onset of a regional dynamic current regime in the newly established North Sea area, as also corroborated by the sudden shift to sandy sediments above the hiatus (Fig. 3(c) and (h)). At this stage, the surrounding paleolandscape was probably flooded and the river valley rims were eroded, which might be reflected by a conspicuously high age of 19 990 cal a BP obtained on an apparently reworked shell. Unfortunately, no stratigraphic control is available for the time span covered by the hiatus, so that the earliest possible date for the establishment of full marine conditions is 9290 cal a BP. According to published sea level curves (Vink *et al.*, 2007), the flooding of the paleolandscape within the study area was completed before 8200 cal a BP.

Above the uppermost sandy layer, 10 to 20 cm-thick layers of well-preserved or fragmented shells and coarser clastic sediments occur in cores GeoB17721-1 and 09-5 (Fig. 3(b) and Fig. 6). These shell layers divide the most recent sediments from the underlying deposits of the first shallow marine phase and are a widespread phenomenon in the shallow North Sea, observed at similar core depths at many sites and are interpreted to be proximal storm layers (Aigner and Reineck, 1982; Uffendorde, 1982). The widespread distribution of such shell layers in the southern North Sea suggests a mega storm/flood event or it might reflect a reorganisation of the current regime induced by the flooding of the Dogger Bank (Fitch *et al.*, 2005).

The uppermost sand packages are commonly referred to as mobile sands that can be mobilised under the influence of recent currents, waves and tides (Zeiler *et al.*, 2000). Coughlan *et al.* (2018) limited this interpretation to the uppermost part of the mobile sands overlying the well-preserved shell layer that obviously is not part of a mobile unit. Accordingly, only the uppermost 30 cm of core GeoB17721-1 above the shell layer are considered here to belong to the mobile sands.

Some implications for recent coastal lowland rivers

The presented study shows that a change in tidal dynamics due to sea level rise can result in a rapid increase of silt deposition and salinisation of coastal lowland rivers. Recent coastal systems in shallow shelf regions are strongly affected by ongoing sea level rise. Silt deposition in tide-influenced waterways, e.g. in the modern Ems River (van Maren *et al.*, 2015) or sea-water intrusions into the river, which might threaten the drinking water supply of cities such as in the Yangtze River Delta (Ye, 2017), are current problems. The high rates of silt deposition and salinisation as demonstrated for the Paleo-Ems River show that such problems can become exacerbated within a few generations. While industrialised countries have the potential to react to changing environmental conditions within decades with proper coastal protection activities, the rapid silt deposition and salinisation of river mouths in coastal environments on century scales is still a persistent issue for developing or threshold countries.

Conclusion

Sediment cores from the infill of the submerged Paleo-Ems valley in the German North Sea reveal the geological record of the transgressional history in this area since the earliest Holocene. Radiocarbon-dated records of changes in sediment grain sizes and the diatom species composition provide new insights into the response of a coastal lowland river to the Holocene transgression and its relationship to the EPV and the surrounding landscape. The onset of the peat growth

in the Paleo-Ems valley was most likely triggered by a sea-level-induced rise of the groundwater table through the link of the Paleo-Ems valley to the EPV. However, peat growth in the Paleo-Ems valley independent from relative sea-level-coupled groundwater, simply as a subject of paludification within local topographic settings, cannot be excluded.

After a period of peat growth lasting for about 1900 years until 9500 cal a BP, the Paleo-Ems valley infill was controlled by brackish environmental conditions. The main finding of this study is that the river was not able to adjust its gradient to the rapidly rising sea level. Thus, the change from freshwater to brackish and finally to marine conditions occurred very rapidly within ~200 years, corresponding to a ~2.5 m sea level rise; well documented in the sedimentological and micropaleontological records. In terms of human timescales, this implies that the river valley silted up within a few generations.

The fate of the Ems paleovalley is exemplary for the evolution of the early Holocene coastal landscape in the German North Sea sector and the rapidly changing world of the Mesolithic hunters and gatherers living there. Humans and fauna directly experienced the drastic changes imposed by deglacial sea level rise. The former fluvial landscape changed rapidly into a coastal landscape with a prograding coastline swallowing the rivers and their levees. Thus, the human population was challenged to respond to these new environmental conditions within a few generations. A rapid increase of silt deposition and salinisation of river mouths in coastal environments on century scales due to sea level rise remains a persistent issue.

Acknowledgements. This research was partly funded through DFG-Research Center/Cluster of Excellence “The Ocean in the Earth System” and the BMWi project “Restrike-XL” (No. 0324231B). We thank Rike Zimmermann who started to work on the peat formation at the 09-x sites, Jürgen Titschack who performed the grain size analyses, and Mareike Höhne who performed the C-S analyses. The study was further supported with data from several anonymous industry partners.

References

- Aigner T, Reineck H-E. 1982. Proximity trends in modern strom sands from the Helgoland Bight (North Sea) and their implications for basin analysis. *Senckenbergiana Maritima* **14**: 183–215.
- Berner RA, Raiswell R. 1984. C/S method for distinguishing freshwater from marine sedimentary rocks. *Geology* **12**: 365–368.
- Blott SJ, Pye K. 2001. GRADISTAT: a grain size distribution and statistics package for the analysis of unconsolidated sediments. *Earth Surface Processes and Landforms* **26**: 1237–1248.
- Clarke J. 2009. Palaeovalley, palaeodrainage, and palaeochannel: what's the difference and why does it matter? *Transactions of the Royal Society of South Australia* **133**: 57–61.
- Coles BJ. 2000. Doggerland: the cultural dynamics of a shifting coastline. *Coastal and Estuarine Environments: Sedimentology, Geomorphology and Geoarchaeology* **175**: 393–401.
- Coughlan M, Fleischer M, Wheeler AJ, Hepp DA, Hebbeln D, Mörz T. 2018. A revised stratigraphical framework for the Quaternary deposits of the German North Sea sector: a geological-geotechnical approach. *Boreas* **47**: 80–105.
- Crosta X, Romero OE, Ther O, Schneider RR. 2012. Climatically-controlled siliceous productivity in the eastern Gulf of Guinea during the last 40 000 yr. *Climate of the Past* **8**: 415–431.
- de Jonge VN, Schuttelaars HM, van Beusekom JEE, Talke SA, de Swart HE. 2014. The influence of channel deepening on estuarine turbidity levels and dynamics, as exemplified by the Ems estuary. *Estuarine, Coastal and Shelf Science* **139**: 46–59.
- Ehlers J 2011. *Das Eiszeitalter*. Spektrum: Heidelberg.

- Figge K. 1980. Das Elbe-Urstromtal im Bereich der Deutschen Bucht (Nordsee). *Eiszeitalter und Gegenwart* **30**: 203–211.
- Fitch S, Thomson K, Gaffney V. 2005. Late Pleistocene and Holocene depositional systems and the palaeogeography of the Dogger Bank, North Sea. *Quaternary Research* **64**: 185–196.
- Gaffney VL, Fitch S, Smith D. 2009. *Europe's lost world: the rediscovery of Doggerland*. Council for British Archaeology: York.
- Hallik R. 1962. Das Elbtal bei Hamburg seit dem Ende der Eiszeit. *Abhandlungen und Verhandlungen des Naturwissenschaftlichen Vereins in Hamburg, Neue Folge* **6**: 233–250.
- Harff J, Bailey GN, Lüth F. 2016. *Geology and archaeology: submerged landscapes of the continental shelf: an introduction*. Geological Society: London; 1–8. *Special Publications*.
- Hartley B. 1996. *An atlas of British diatoms*. Biopress: Bristol.
- Hempel L. 1963. Über morphologische Formengruppen der Erosion an der Ems: Beiträge zur Quartärgeologie und Morphologie Westfalens. *Eiszeitalter und Gegenwart - Quaternary Science Journal* **14**: 68–76.
- Hepp DA, Hebbeln D, Kreiter S, Keil H, Bathmann C, Ehlers J, Mörz T. 2012. An east-west-trending Quaternary tunnel valley in the south-eastern North Sea and its seismic-sedimentological interpretation. *Journal of Quaternary Science* **27**: 844–853.
- Hepp DA, Warnke U, Hebbeln D, Mörz T. 2017. Tributaries of the Elbe-Palaeovalley: features of a hidden palaeolandscape in the German Bight, North Sea. In *Under the Sea: archaeology and palaeolandscapes of the continental shelf*, Bailey GN, Harff J, Sakellariou D (eds). Springer, 211–222.
- Hjelstuen BO, Sejrup HP, Valvik E, Becker LWM. 2017. Evidence of an ice-dammed lake outburst in the North Sea during the last deglaciation. *Marine Geology*.
- Jelgersma S 1961. *Holocene sea level changes in the Netherlands*. van Aelst: Maastricht.
- Lange W, Menke B. 1967. Beiträge zur frühpostglazialen erd- und vegetationsgeschichtlichen Entwicklung im Eidergebiet, insbesondere zur Flussgeschichte und zur Genese des sogenannten Basistorfes. *Meyniana* **17**: 29–44.
- Meyer K-D. 1983. Zur Anlage der Urstromtäler in Niedersachsen. *Zeitschrift für Geomorphologie, Neue Folge* **27**: 147–160.
- Morse JW, Berner RA. 1995. What determines sedimentary C/S ratios? *Geochimica et Cosmochimica Acta* **59**: 1073–1077.
- Nicholls RJ, Cazenave A. 2010. Sea-level rise and its impact on coastal zones. *Science* **328**: 1517–1520.
- Özmaral A 2017. *Climatically controlled sedimentary processes on continental shelves*. Ph.D. thesis. University of Bremen: Bremen.
- Peeters JHM, Cohen KM. 2014. Introduction to North Sea submerged landscapes and prehistory. *Netherlands Journal of Geosciences - Geologie en Mijnbouw* **93**: 1–3.
- Phillips E, Hodgson DM, Emery AR. 2017. The Quaternary geology of the North Sea basin. *Journal of Quaternary Science* **32**: 117–126.
- Phillips E, Cotterill C, Johnson K, Crombie K, James L, Carr S, Ruiter A. 2018. Large-scale glactectonic deformation in response to active ice sheet retreat across Dogger Bank (southern central North Sea) during the Last Glacial Maximum. *Quaternary Science Reviews* **179**: 24–47.
- Romero OE, Armand LK. 2010. Marine diatoms as indicators of modern changes in oceanographic conditions. In *The diatoms: applications for the environmental and earth sciences*, Stoermer EF, Smol JP (eds). Cambridge University Press: Cambridge; 373–400.
- Round FE, Crawford RM, Mann DG. 1990. *The diatoms: biology and morphology of the genera*. Cambridge University Press: Cambridge.
- Schrader H, Gersonde R. 1978. Diatoms and silicoflagellates. *Utrecht Micropaleontological Bulletins* **17**: 129–176.
- Scourse JD, Wanamaker AD, Weidman C, Heinemeier J, Reimer PJ, Butler PG, Witbaard R, Richardson CA. 2012. The marine radiocarbon bomb pulse across the temperate North Atlantic: A compilation of $\Delta^{14}\text{C}$ time histories from Arctica Islandica growth increments. *Radiocarbon* **54**: 165–186.
- Streif H, Uffenorde H, Vinken R 1983. *Untersuchungen zum pleistozänen und holozänen Transgressionsgeschehen im Bereich der südlichen Nordsee: Abschlußbericht zum DFG-Forschungsvorhaben*. Internal report 95306. Niedersächsisches Landesamt für Bodenforschung: Hannover.
- Stuiver M, Reimer PJ. 1993. Extended ^{14}C data base and revised CALIB 3.0 ^{14}C age calibration. *Radiocarbon* **35**: 215–230.
- Tietze G 1983. *Das Jungpleistozän und marine Holozän nach seismischen Messungen nordwestlich Eiderstedt/Schleswig-Holstein*. Ph.D. thesis. Christian-Albrechts-Universität: Kiel.
- Uffenorde H. 1982. Zur Gliederung des klastischen Holozäns im mittleren und nordwestlichen Teil der Deutschen Bucht (Nordsee) unter besonderer Berücksichtigung der Foraminiferen. *Eiszeitalter und Gegenwart - Quaternary Science Journal* **32**: 177–202.
- van Maren DS, van Kessel T, Cronin K, Sittoni L. 2015. The impact of channel deepening and dredging on estuarine sediment concentration. *Continental Shelf Research* **95**: 1–14.
- Vink A, Steffen H, Reinhardt L, Kaufmann G. 2007. Holocene relative sea-level change, isostatic subsidence and the radial viscosity structure of the mantle of northwest Europe (Belgium, the Netherlands, Germany, southern North Sea). *Quaternary Science Reviews* **26**: 3249–3275.
- Warnke U, Hepp DA, Mörz T. 2014. An der Mündung der Urems. *Spektrum der Wissenschaft* **14**: 16–18.
- Wolters S, Zeiler M, Bungenstock F. 2010. Early Holocene environmental history of sunken landscapes: pollen, plant macrofossil and geochemical analyses from the Borkum Riffgrund, southern North Sea. *International Journal of Earth Sciences* **99**: 1707–1719.
- Ye Y-c. 2017. *Marine Geo-Hazards in China*. Elsevier: Amsterdam.
- Zeiler M, Schulz-Ohlberg J, Figge K. 2000. Mobile sand deposits and shoreface sediment dynamics in the inner German Bight (North Sea). *Marine Geology* **170**: 363–380.